Landfast ice affects the stability of the Arctic halocline: evidence from a numerical model

Polona Itkin[1], Martin Losch[1], Rüdiger Gerdes[1]

Corresponding author: P. Itkin, Sea Ice Physics, Alfred Wegener Institute Helmholtz Center for Polar and Marine Research, Bussestrasse 24, 27570 Bremerhaven, Germany. (Polona.Itkin@awi.de)

[1]Alfred Wegener Institute, Helmholtz Centre for Polar and Marine Research, Bremerhaven, Germany.

Abstract.

Landfast ice covers large surface areas of the winter Siberian Seas. The immobile landfast ice cover inhibits divergent and convergent motion, hence dynamical sea ice growth and re-distribution, decouples winter river plumes in coastal seas from the atmosphere and positions polynyas at the landfast ice edge offshore. In spite of the potentially large effects, state-of-the-art numerical models usually do not represent landfast ice in its correct extent. A simple parametrization of landfast ice based on bathymetry and internal sea ice strength is introduced its effects on the Arctic Ocean are demonstrated. The simulations suggest that the Siberian landfast ice impacts the Arctic halocline stability through enhanced brine production in polynyas located closer to the shelf break and by re-directing river water to the Canadian Basin. These processes strengthen the halocline in the Canadian Basin, but erode its stability in the Makarov and Eurasian Basin.

1. Introduction

One of the dominant characteristics of the winter Arctic shelf seas is landfast ice (also land-fast, fast or shore-fast ice), sea ice that is immobile and mechanically fastened to the coast or to the sea floor. As there is no compressive deformation, landfast ice grows only thermodynamically and rarely exceeds thicknesses of 1.5 m [*Romanov*, 2004]. It can extend a few (Beaufort Sea, Chukchi Sea, Western Laptev Sea) to several hundred kilometers from the coast into the ocean (Kara Sea, Eastern Laptev Sea, East Siberian Sea, see Fig. 1). The mechanisms that determine the landfast ice formation, extent and decay are not fully understood. To complicate things further, these mechanisms differ regionally. In the Chukchi and Beaufort Sea the landfast ice edge is found at relatively shallow depth of 18 m [*Mahoney et al.*, 2007], while on the Eurasian shelf this depth is between 25 and 30 m [*Dmitrenko et al.*, 2005a; *Proshutinsky et al.*, 2007]. In the Chukchi and Beaufort Sea the landfast ice is immobilized behind a row of bottom reaching pressure ridges [*Mahoney et al.*, 2007]. In the Kara Sea the landfast ice is formed behind a row of small islands parallel to the coast [*Divine et al.*, 2004]. At the landfast ice edge in the Laptev and East Siberian Seas grounded pressure ridges are rare [*Reimnitz et al.*, 1994; *Eicken et al.*, 2005]. *Proshutinsky et al.* [2007] proposed that the landfast ice edge occurs where the warm intermediate Atlantic water reaches the surface after upwelling at the shelfbreak. *König Beatty and Holland* [2010] attributed the landfast ice extent to the mechanical properties of the sea ice. Strong freshwater and brackish sea ice [*Dethleff et al.*, 1993; *Eicken et al.*, 2005] formed in low salinity shelf seas with high river water content might ground at wide and shallow sand banks [*Dethleff et al.*, 1993; *Reimnitz* *et al.*, 1994] and from there extend with long tongues toward the landfast ice edge. Tides in the region are very weak and the tidal amplitudes of up to 10 cm in the Southeastern Laptev Sea *Fofonova et al.* [2014] might not be large enough to deform the extensive landfast ice cover.

Especially in the Siberian Seas, where landfast ice has the largest extent, it is thought to have three roles:

1. Landfast ice limits the sea ice thickness by preventing sea ice compression (e.g. pressure ridges) in convergent motion of sea ice. By the same token it lowers the sea ice production by preventing sea ice divergence and lead formation. If these processes are not adequately represented in a numerical model, simulated thickness fields are not realistic [*Johnson et al.*, 2012].

2. An immobile lid of the landfast ice effectively decouples the inner shelf from the atmosphere and affects the river water distribution. The seasonal runoff of the large Siberian rivers (Ob, Lena, Yenisei) determines the water masses of the shallow Siberian shelf. In a summer with strong onshore winds large parts of the summer maximal discharge can be held back on the inner shelf until winter [*Dmitrenko et al.*, 2005b]. The large amount of the fresh river water in the Arctic surface layer enhances the ocean stratification.

3. The extent of landfast ice determines the areas of low sea ice concentration—so called flaw polynyas (also flaw lead polynyas or flaw leads)—along the landfast ice edge during offshore wind conditions. The water in these polynyas is more saline than directly at the coast, where ocean salinities remain low due to fresh river water inflow and consequently more brine is rejected during sea ice production. The brine formed in the winter shelf seas maintain, along with the cool water formed by winter convection north of the Barents

Sea [*Rudels et al.*, 1996], the Arctic halocline [*Aagaard et al.*, 1981; *Martin and Cavalieri*, 1989; *Cavalieri and Martin*, 1994; *Winsor and Björk*, 2000]. The cold and saline water flows off the shelves and sinks along the shelf break where it feeds into the halocline layer (Fig. 2), which decouples the cold Arctic surface layer from the warm intermediate-depth Atlantic layer. The surface layer stays cold with temperatures close to the freezing point due to a seasonal sea ice melting - freezing cycle and the layer is fresh due to a strong river runoff. In contrast, the ocean temperature at mid-depth is up to several degrees above zero. This warm and saline Atlantic water enters the ocean through the Nordic Seas (Fig. 1).

Landfast ice has been found important for the accurate simulation of the sea surface height [*Proshutinsky et al.*, 2007] and sea ice thickness *Johnson et al.* [2012]. Although landfast ice is also important for the processes maintaining the Arctic halocline, it is usually not properly represented in state-of-the-art sea ice-ocean models. In this study we demonstrate the effects of the landfast ice for the Arctic halocline.

The outline of this paper is as follows. In section 2 we describe the numerical model for the sensitivity study. In Section 2.1 we describe the details of the landfast ice parametrization. In sections 3, 4 and 5 we present and discuss our results. A summary of our findings and final remarks are given in section 6.

2. Model setup

Our model is a regional coupled sea ice - ocean model based on the Massachusetts Institute of Technology General Circulation Model code - MITgcm [*Marshall et al.*, 1997; *MITgcm Group*, 2014] with a model domain covering the Arctic Ocean, Nordic Seas and northern North Atlantic. The horizontal resolution of is $1/4^{\circ}$ ($\sim$28 km) on a rotated grid with the grid equator passing through the geographical North Pole. The model has 36 vertical levels unevenly distributed in a way that the surface layer is well resolved at the cost of the poor resolution in the deep layer. The shelf bottom topography has realistic details that allow dense brine to flow downslope and off the shelf. Vertical mixing in the ocean is parameterized by a K-Profile Parameterization (KPP) scheme [*Large et al.*, 1994] and tracers (temperature and salinity) are advected with an unconditionally stable seventh-order monotonicity preserving scheme [*Daru and Tenaud*, 2004] that requires no explicit diffusivity. The sea ice model is a dynamic-thermodynamic sea-ice model with a viscous-plastic rheology [*Losch et al.*, 2010]. The model has a non-linear free surface and sea ice that depresses the surface ocean layer according to its mass. We avoid numerical issues associated with too thin surface layers when ice gets very thick by using a rescaled vertical z*-coordinate [*Campin et al.*, 2008] that distributes the excursion of the free sea surface between all vertical levels to the bottom. The same model set-up has been used by *Itkin et al.* [2013] except that now the vertical background diffusivity has been lowered to 10^{-6} m^2/s as recommended by *Nguyen et al.* [2009] to achieve a better defined Arctic halocline.

The model is initialized by the PHC climatology [*Steele et al.*, 2001] and has initially no sea ice cover. For a spin-up we run the model for 30 years forced by the atmospheric climatology of the Coordinated Ocean Research Experiment (CORE) version 2 based on a reanalysis of the National Center for Atmospheric Research/National Centers for Environmental Prediction (NCAR/NCEP) [*Large and Yeager*, 2009]. Subsequently the model is driven from 1948 to 1978 by daily atmospheric data also provided by CORE. Our model experiments start in 1979 and continue until 2010. They are forced by the atmospheric reanalysis – The Climate Forecast System Reanalysis (NCEP–CFSR) [*Saha et al.*, 2010]. Surface salinity in ice free regions is restored to a mean salinity field (PHC climatology) with a time scale of 180 days to avoid model drift. River runoff was treated like a surface volume flux and it was prescribed for the main Arctic rivers according to the Arctic Ocean Model Intercomparison Project (AOMIP, http://www.whoi.edu/projects/AOMIP/) protocol. Open boundaries are formulated following *Stevens* [1991]; they are located at 50°N in the Atlantic and just south of the Bering Strait. Temperature and salinity at the open boundaries are taken from the PHC climatology. The Barents Strait inflow is prescribed as 0.8 Sv and the stream function at open boundary in the Atlantic Ocean derived from a North Atlantic simulation [*Gerdes and Köberle*, 1995] and modified to balance the net volume flow in the model domain.

2.1. Landfast ice Parameterization

The mechanisms that determine the landfast ice formation and extent depend of the specific region and are not fully understood. There have been many attempts to model or parameterize landfast ice. *Lieser* [2004] developed a parameterization based on the ratio of sea ice thickness and total water column depth. For a specified threshold ratio the grid cells assigned as landfast ice remained at rest and surface momentum flux into the ocean was set to zero. His approach in a 1/4° (28 km) model resulted in too thick landfast ice that even survived the summer. A similar procedure was used in higher horizontal resolution models (3-12 km) by *Johnson et al.* [2012] and *Rozman et al.* [2011]. Both studies use prescribed landfast ice areas obtained from bathymetrical limits or observations. In the Kara Sea, where the landfast ice forms over deep waters behind a row of coastal islands, *Olason* [2012] successfully modeled landfast ice by adjusting the internal sea ice strength parameters in the viscous-plastic rheology of *Hibler* [1979].

Our model grid does not resolve small islands and shallow topographical features in the Siberian Seas, where the landfast ice might get grounded. Therefore we designed a simplified and uniform parametrization based on *König Beatty and Holland* [2010] that takes into account water column depth and landfast ice internal strength. The latter is justified by a sharp salinity gradient between the shallow shelf waters of the Kara, Laptev and East Siberian Sea and the deep ocean. In 1992, *Dethleff et al.* [1993] documented freshwater ice up to 100 km seaward off the Lena Delta. In 1999 the freshwater and brakish sea ice with salinity below 1 was confined to the coastal waters adjacent to the eastern Lena Delta with water depth less than 10 m, while river water on average still contributed 62 % of the landfast ice further offshore in the southeastern Laptev Sea [*Eicken et al.*, 2005]. .

In the widely used sea ice strength parametrization (e.g. *Hibler* [1979]; *Zhang and Hibler III* [1997]) compressive strength P depends just on the sea ice thickness h and concentration A:

$$P = P^* h \exp(-C^*(1-A)), \tag{1}$$

where the empirical sea ice strength parameters, $P^* = 2750 N/m^2$ and $C^* = 20$ are constants.

The landfast ice parametrization used in this study takes into account the unresolved shallow topographical features inside the maximal landfast ice edge mark (25 m) and increased sea ice internal strength attributed to the lower sea ice salinity in the same area by setting the P^* to the double of the drift ice. Such landfast ice would still fail under strong offshore wind if the distance between the coastline and 25-m-bathymetrical boundary is large. To prevent this we amended the sea ice rheology in the regions shallower than 25 m with sea ice tensile strength T following *König Beatty and Holland* [2010]:

$$\zeta = \frac{P+T}{2\Delta}, \tag{2}$$

$$\eta = \frac{P+T}{2\Delta e^2} = \zeta / e^2, \tag{3}$$

and

$$p = P - T, \tag{4}$$

where ζ is bulk viscosity, η is shear viscosity, $e = 2$ is eccentricity constant and p is the pressure term. This moves the elliptical yield curve in the principal stress space into the I. quadrant, when the water column is shallower than 25 m and leaves the curve unmodified otherwise. $T = \frac{P}{2}$, which is consistent with the estimates by *Tremblay and Hakakian* [2006].

For the sensitivity study we compare a control run (CTRL) and a landfast ice run (LF) that differ only in this additional landfast ice parameterization.

3. Impact of the landfast parameterization on the sea ice

In the Laptev and East Siberian Sea the landfast ice cover forms in December, reaches its maximal extent in April, breaks up into fully drifting ice in May or June and melts in summer. Starting in May, the atmospheric temperatures are too warm to have a significant amount of brine produced in the polynya. Hence, in this study we define wintertime as the months December to April. In our model landfast ice breaks up completely in early summer. At atmospheric temperatures above zero and when A drops below 1, sea ice looses its internal strength exponentially making P^* irrelevant, because P depends exponentially on A.

If we define coastal sea ice with drift speeds below 1 mm/s as landfast ice, then the parametrization in LF comparing to CTRL leads to substantially larger areas of landfast ice in April, during the annual maximal extent (Figure 3 panels a and b). The simulated landfast ice is slow enough for polynyas to form at its seaward edge (Figure 3 c and d). The 1 mm/s contour and polynyas in LF agree better with the 1997-2006 landfast ice edge produced by the Arctic and Antarctic Research Institute, Saint Petersburg, Russia (*Smolyanitsky et al.* [2007], hereafter AARI dataset). In LF, however, the Laptev Sea polynya is located too far away from the coast. This might be a consequence of the coarse model resolution and the high P^* value. In the Kara Sea our parametrization has only a minor effect because the shelf sea ice is much deeper than the 25 m threshold we use in the parametrization and the small offshore islands there are located in areas where the surrounding seas exceed the depth of 150 m.

The effect of the parametrization is clearly visible in the sea ice thickness maps (Fig. 4). LF sea ice is by up to 30 cm thinner under the regions affected by the landfast ice parametrization in the Kara, Laptev, East Siberian, Chukchi and Beaufort Seas. The difference pattern accurately matches the landfast ice extent from the AARI dataset (Fig. 3). The largest negative differences are in the polynya at the landfast ice edge in the East Siberian and Laptev Seas, while in the coastal regions of the Laptev Sea differences are positive to reflect the erroneous polynya location in the CTRL.

The thinner sea ice in the landfast ice area in LF is a consequence of exclusive thermodynamic sea ice growth. The thermodynamical growth itself is also different between the runs (Fig. 4): in both cases the highest growth rates occur in the polynyas. In LF this is further offshore than in CTRL.

As a volume of water is thermodynamically turned into sea ice, salt is expelled from this volume and remains in the ocean. Because this process increases the salinity in the surface ocean, one can define a 'virtual salt flux' $S_{flux} = FW_{flux}S$, where FW_{flux} is freshwater flux and S is the salinity of the surface water minus 4 where the salinity is equal or higher than 4. This approximates the constant sea ice salinity of 4 in our model. The resulting S_{flux} differences resemble the difference pattern in the thermodynamic growth (Fig. 4). Because S_{flux} depends also on the sea surface salinity its is relatively low in the East Siberian Sea although the sea ice production there is high. S_{flux} is an order of magnitude higher and opposite in sign compared to the virtual salt flux generated by the sea surface salinity restoring (not shown). Salinity is only restored to climatology in the ice free part of the model grid cell.

The largest differences in the winter sea ice cover between the runs are found in the Laptev and East Siberian Seas. This is the area with the greatest landfast ice extent over the shallow shelf and hence our parametrization has the largest effect there. In time series, we compare the contributions of wintertime sea ice concentration, thickness, sea ice production, ocean surface salinity and S_{flux} to wintertime dense shelf water production in both simulations (Fig. 5). The mean sea ice concentration over the Siberian Seas is high and very similar in both simulations. This is not surprising as the differences between the runs are mainly in the positioning of the polynyas within the Siberian Seas. The sea ice concentrations are a little lower in CTRL as the drifting sea ice allows more small leads. Sea ice is about 10 cm thinner in LF than in CTRL. This is a consequence of less ridging through convergent motion in the landfast ice area and less advection of sea ice into the region. In contrast, there is more thermodynamically grown sea ice in LF. While the polynyas in LF are shifted offshore into more saline sea water, a higher fraction of fresh river water reduces the salinity in the shelf seas. Towards the end of the runs these counteracting effect leads to a similar surface salinity in polynyas in both runs. Still, higher sea ice production leads to higher S_{flux} in LF.

The differences in the sea ice production and S_{flux} between CTRL and LF are geographically distributed as expected so that we conclude that this sensitivity study can be used to estimate the importance of the landfast ice for the Arctic Ocean halocline stability.

4. Impact of the landfast parameterization on the Arctic halocline

In this section we compare the end of winter (April) climatologies (2000-2010) because of the high seasonality of the mixed layer depth in the Arctic. First we examine the buoyancy, $b = -g\frac{\rho-\rho_0}{\rho_0}$ at the top of the halocline (25 – 30 m). The differences between LF and CTRL show regional effects of the landfast ice parametrization with less buoyancy in LF in the Canadian Basin and more buoyancy centered in Makarov and Eurasian Basins (Fig. 6a and b).

To understand the relevance of these differences to the water column stability we examine three oceanographic sections; each section runs through one of the major Arctic basins: Canadian, Makarov and Eurasian as shown on Fig. 1 and 6. In the first section running from the Eurasian coast over the Wrangel Island to the Ellesmere Island (Fig. 7) there is increased salinity by locally up to 0.6 at the halocline layer in LF (25 – 30 m), while the surface layer tends to be fresher than in CTRL. Especially in the surface layer, the differences are not homogeneous and locally have alternating signs. Along with the increased temperature at the top halocline depth this suggests this layer is fed by relatively warm shelf bottom water mixed with brine originating from the sea ice production. This influence is supported by the Hovmöller diagrams of differences at the section across the pathway of the water masses from the East Siberian Sea to the Canadian Basin (Fig. 8 a and b). In LF, this shelf water has continuously larger salinity at the halocline depth (panel a), while the surface layer is typically fresher which generally is associated with higher river water content (panel b). The salinity and river water fraction in the surface layer differences are not constant in time. Notably the salinity difference is positive in the early 1990s and in the mid 2000s. Both events are accompanied with a negative difference in river water fraction. The differences in temperature and salinity described above have consequences for the stratification. The buoyancy frequency N^2 is larger in LF than in CTRL pointing to a higher stability at the winter mixed layer depth.

In contrast, the second section which runs from East Siberian Sea to the Northern Greenland (Fig. 9) shows a different pattern with higher salinities by up to 0.8 in the surface layer that reflects a decreased river water content in LF compared to CTRL. The salinity at the depth of the halocline only increases only by about 0.1, such that the overall stability of the upper halocline is reduced. The third section runs from the Laptev Sea to the Fram Strait (Fig. 10). Here the differences between the runs are similar as in the second section, but not as pronounced. While there is still less river water in the surface layer, the halocline layer has more river water in LF than in CTRL. Here, the landfast ice parametrization has no clear effect on the halocline stability. This is again supported by the Hovmöller diagrams of differences at the section across the pathway of shelf water from the Laptev Sea (Fig. 8 c and d). In LF, the surface layer is mostly more saline, while the time series of the river water fraction differences show a strong seasonal cycle with typically less river water in the surface layer in the winter and more in the summer (not shown).

5. Discussion

Landfast ice simulated in LF grows almost exclusively thermodynamically and allows very little ice production due to convergent motion (dynamical sea ice growth). Therefore the coastal regions covered by landfast ice in LF are thinner than in CTRL. To some extent, the arbitrary choice of the 25 m isobath for turning on the parameterization place the polynyas in the approximately observed positions.In contrast, in CTRL polynyas are located directly on the coast. The shift of the polynyas from the coast in CTRL toward a realistic landfast ice edge location in LF moves the brine production closer to the shelfbreak and into more saline ocean where more brine is produced per sea ice volume.

To determine if the amount of brine produced in our simulations is realistic we first compare the available sea ice production estimates for the Laptev Sea. In LF during 2000s a mean of 144 km^3 of sea ice is produced per winter (not shown, but Fig. 5a shows winter sea ice production for the East Siberian and Laptev Sea, roughly half of which is produced in that Laptev Sea. That is above *Rabenstein et al.* [2013]'s estimate of $94{\pm}27 km^3$ for the southeastern Laptev Sea for winter (late December till mid-April) 2007/2008. *Willmes et al.* [2011] estimate a lower $55{\pm}15$ km^3 for the entire Laptev Sea during winter, but these authors only took into account ice production in areas with sea ice thinner than 20 cm.

Our results indicate that with an appropriate representation of landfast ice more river water is stored in the Siberian Seas. While in CTRL more river water is dispersed by the wind acting through the drifting sea ice, in LF this river water is protected from the wind by the immobile shield of the landfast ice and remains on the shelf. From there the river water plume is driven northeastward by geostrophic currents (black arrows on Fig. 1) into the Canadian Basin and less river water reaches other parts of the Arctic. In LF, in summers with strong offshore winds the increased amounts of the river water stored on the shelf during the winter are driven northwards into the European and Makarov Basins. Still, these river water pulses do not change the sign of the salinity differences in the surface layer and and do not affect the halocline stability.

The combined effect of increased brine export to the Central Arctic and redistribution of the river water from the winter shelf in LF compared to the CTRL changes the buoyancy at the Arctic halocline. In the Canadian Basin the surface layer freshens locally due to increased river water content as a consequence of the landfast ice parametrization, while the halocline layer becomes saltier due to the difference in the brine production in the Siberian polynyas. Both surface and halocline depth differences make the halocline in LF stronger. Our simulation supports *Nguyen et al.* [2012]'s conclusions that the Canadian Basin halocline is maintained by the dense water formed on the Eurasian shelf.

In the Makarov and Eurasian Basin the difference signal is dominated by the increase in the surface salinity that is again the consequence of the redirection of the river water to the Canadian Basin. Consequently the already weak halocline in this sector of the Arctic [*Boyd et al.*, 2002; *Rudels et al.*, 2004] is further eroded in LF. The effect of the landfast ice resembles that of the Great salinity anomaly [*Steele and Boyd*, 1998; *Johnson and*

Polyakov, 2001] observed in the early 1990s, where the changes in the wind circulation enhanced the river water export to the Canadian Basin and increased brine production in the Siberian Seas polynyas that eroded the Arctic halocline over substantial parts of the Arctic Ocean. During the Great salinity anomaly and similarly also in the mid 2000s landfast ice in LF has an effect outweighing the anomalous offshore winds and the differences in surface salinity and river water content of the shelf waters originating form the East Siberian Sea during these two periods change the sign (Fig. 8a and b).

Yu et al. [2014] detected a general decrease of the Arctic landfast ice extent of 7±1.5 % per decade in the period from 1976 till 2007. In the Chukchi, Laptev and East Siberian Seas also the landfast ice season is getting shorter, reflecting the general negative trend in the summer sea ice extent in the Siberian Seas [*Comiso et al.*, 2008; *Stroeve et al.*, 2012]. According to our results this trend should have implications for the halocline stability. The reduction in the extent and duration in the Siberian Seas would lead to a weaker halocline in the Canadian Basin, but conversely also to a stronger halocline in the Makarov and and Eurasian Basins. Especially for the latter two basins the Atlantic water layer has been reported to be warming [*Polyakov et al.*, 2010]. In such a case, the loss of the landfast ice would inhibit the heat transport from the Atlantic Water layer to the surface and delay the further rapid sea ice loss in the Arctic.

6. Summary and conclusions

An accurate representation of the landfast ice in a sea ice-ocean coupled model has an impact not only on the winter sea ice and brine production but also on the river water distribution. The landfast ice in the LF shields the river water that remains on the shelf in winter from the winds and promotes northeastward flow of the river water with the coastal currents. We have been able to show this in a sensitivity study with a simple-to-implement landfast ice parametrization that generated landfast ice over extensive areas of the Laptev and East Siberian Seas. In LF more river water reaches the Canadian Basin and less the Makarov and Eurasian Basin. Also the polynyas are located closer to the shelf break. From there more brine reaches the halocline depth of the Canadian Basin. The surface salinity decrease due to the river water and the halocline salinity increase due to the brine both strengthen the halocline in the Canadian Basin, whereas in the Makarov and Eurasian Basins the surface salinity increase erodes the already low halocline stability. Consequently in the latter two basins where the Atlantic water layer is still relatively warm and the halocline is already eroded, extensive landfast ice further weakens the halocline and promotes entraining Atlantic water into the ocean mixed layer that might lead to sea ice melt.

Based on our simulations we recommend to include our landfast ice parametrization to those regional numerical models that address the halocline stability and shelf - deep basin exchanges. The stratification modified by brine produced in the polynyas and the river water that supplies the Arctic Ocean with sediments, nutrients, and pollutants are key factors for biogeochemical processes.

Acknowledgments. We would like to thank Valeria Selyuzhenok, Alfred Wegener Institute for her help with the observational data comparison. We are grateful to Karel Castro-Morales and Kathrin Riemann-Campe, also Alfred Wegener Institute who have contributed to the model development. Polona Itkin's PhD studies have been partially supported by a grant of the Municipality of Ljubljana, Slovenia.

References

Aagaard, K., L. Coachman, and E. Carmack (1981), On the halocline of the Arctic Ocean, *Deep Sea Research Part A. Oceanographic Research Papers*, *28*(6), 529–545.

Boyd, T. J., M. Steele, R. D. Muench, and J. T. Gunn (2002), Partial recovery of the Arctic Ocean halocline, *Geophysical Research Letters*, *29*(14), 2–1–2–4, doi:10.1029/2001GL014047.

Campin, J., J. Marshall, and D. Ferreira (2008), Sea ice-ocean coupling using a rescaled vertical coordinate z*, *Ocean modelling*, *24*(1-2), 1–14.

Cavalieri, D., and S. Martin (1994), The contribution of Alaskan, Siberian, and Canadian coastal polynyas to the cold halocline layer of the Arctic Ocean, *Journal of Geophysical Research-Oceans*, *99*(C9).

Comiso, J., C. Parkinson, R. Gersten, and L. Stock (2008), Accelerated decline in the Arctic sea ice cover, *Geophys. Res. Lett*, *35*(1), L01,703.

Daru, V., and C. Tenaud (2004), High order one-step monotonicity-preserving schemes for unsteady compressible flow calculations, *JOURNAL OF COMPUTATIONAL PHYSICS*, *193*(2), 563–594, doi:10.1016/j.jcp.2003.08.023.

Dethleff, D., D. Nürnberg, and E. Groth (1993), East siberian arctic region expedition'92: the laptev sea: its significance for arctic sea-ice formation and transpolar sediment flux/by d. dethleff..., *Berichte zur Polarforschung (Reports on Polar Research)*, *120*.

Divine, D., R. Korsnes, and A. Makshtas (2004), Temporal and spatial variation of shore-fast ice in the Kara Sea, *Continental Shelf Research*, *24*(15), 1717–1736.

Dmitrenko, I., K. Tyshko, S. Kirillov, H. Eicken, J. Hölemann, and H. Kassens (2005a), Impact of flaw polynyas on the hydrography of the Laptev Sea, *Global and planetary* *change*, *48* (1-3), 9–27.

Dmitrenko, I., S. Kirillov, H. Eicken, and N. Markova (2005b), Wind-driven summer surface hydrography of the eastern siberian shelf, *Geophysical research letters*, *32* (14), L14,613.

Eicken, H., I. Dmitrenko, K. Tyshko, A. Darovskikh, W. Dierking, U. Blahak, J. Groves, and H. Kassens (2005), Zonation of the Laptev Sea landfast ice cover and its importance in a frozen estuary, *Global and planetary change*, *48* (1-3), 55–83.

Fofonova, V., A. Androsov, S. Danilov, M. Janout, E. Sofina, and K. Wiltshire (2014), Semidiurnal tides in the laptev sea shelf zone in the summer season, *Continental Shelf Research*, *73* (0), 119 – 132, doi:http://dx.doi.org/10.1016/j.csr.2013.11.010.

Gerdes, R., and C. Köberle (1995), On the influence of DSOW in a numerical model of the North Atlantic general circulation, *Journal of Physical Oceanography*, *25*, 2624–2642, doi:doi: 10.1175/1520-0485(1995)025¡2624:OTIODI¿2.0.CO;2.

Hibler, W. (1979), A dynamic thermodynamic sea ice model, *Journal of Physical Oceanography*, *9* (4), 815–846.

Itkin, P., M. Karcher, and G. R. (2013), Is weaker Arctic sea ice changing the Atlantic water circulation?, *Journal of Geophysisical Research*, *submitted*.

Johnson, M., and I. Polyakov (2001), The Laptev Sea as a source for recent Arctic Ocean salinity changes, *Geophys. Res. Lett*, *28* (10), 2017–2020.

Johnson, M., A. Proshutinsky, Y. Aksenov, A. T. Nguyen, R. Lindsay, C. Haas, J. Zhang, N. Diansky, R. Kwok, W. Maslowski, S. Haekkinen, I. Ashik, and B. de Cuevas (2012), Evaluation of Arctic sea ice thickness simulated by Arctic Ocean Model Intercomparison Project models, *JOURNAL OF GEOPHYSICAL RESEARCH-OCEANS*, *117*, doi:

10.1029/2011JC007257.

König Beatty, C., and D. M. Holland (2010), Modeling landfast sea ice by adding tensile strength, *Journal of Physical Oceanography*, *40*(1), 185–198.

Large, W., and S. Yeager (2009), The global climatology of an interannually varying air-sea flux data set, *Climate Dynamics*, *33*(2-3), 341–364, doi:10.1007/s00382-008-0441-3.

Large, W. G., J. C. McWilliams, and S. C. Doney (1994), Oceanic vertical mixing: A review and a model with a nonlocal boundary layer parameterization, *Reviews of Geophysics*, *32*(4), 363–403, doi:10.1029/94RG01872.

Lieser, J. (2004), A numerical model for short-term sea ice forecasting in the Arctic= Ein numerisches Modell zur Meereisvorhersage in der Arktis, *Berichte zur Polar-und Meeresforschung= Reports on polar and marine research*, *485*, 93.

Losch, M., D. Menemenlis, J.-M. Campin, P. Heimbach, and C. Hill (2010), On the formulation of sea-ice models. part 1: Effects of different solver implementations and parameterizations, *Ocean Modelling*, *33*(1), 129–144.

Mahoney, A., H. Eicken, A. Gaylord, and L. Shapiro (2007), Alaska landfast sea ice: Links with bathymetry and atmospheric circulation, *J. Geophys. Res*, *112*, C02,001.

Marshall, J., A. Adcroft, C. Hill, L. Perelman, and C. Heisey (1997), A finite-volume, incompressible Navier Stokes model for studies of the ocean on parallel computers, *J. geophys. Res*, *102*(C3), 5753–5766.

Martin, S., and D. Cavalieri (1989), Contributions of the Siberian Shelf Polynyas to the Arctic Ocean intermediate and deep water, *Journal of Geophysical Research*, *94*(C9).

MITgcm Group (2014), MITgcm User Manual, *Online documentation*, MIT/EAPS, Cambridge, MA 02139, USA, http://mitgcm.org/public/r2_manual/latest/online_documents.

Nguyen, A. T., D. Menemenlis, and R. Kwok (2012), Source and pathway of the Western Arctic upper halocline in a data-constrained coupled ocean and sea ice model, *Journal of Physical Oceanography*, *42*, 802–823, doi:10.1175/JPO-D-11-040.1.

Nguyen, A. T., D. Menemenlis, and R. Kwok (2009), Improved modeling of the Arctic halocline with a subgrid-scale brine rejection parameterization, *JOURNAL OF GEOPHYSICAL RESEARCH-OCEANS*, *114*, doi:10.1029/2008JC005121.

Olason, E. Ö. (2012), Dynamical modelling of kara sea land-fast ice, Ph.D. thesis, University of Hamburg.

Polyakov, I., L. Timokhov, V. Alexeev, S. Bacon, I. Dmitrenko, L. Fortier, I. Frolov, J.-C. Gascard, E. Hansen, V. Ivanov, S. Laxon, C. Mauritzen, D. Perovich, S. K., S. H., V. Sokolov, M. Steele, and J. Toole (2010), Arctic ocean warming contributes to reduced polar ice cap, *Journal of Physical Oceanography*, *40*, 2743–2756, doi: 10.1175/2010JPO4339.1.

Proshutinsky, A., I. Ashik, S. Häkkinen, E. Hunke, R. Krishfield, M. Maltrud, W. Maslowski, and J. Zhang (2007), Sea level variability in the Arctic Ocean from AOMIP models, *Journal of Geophysical Research*, *112*(C4), C04S08.

Rabenstein, L., T. Krumpen, S. Hendricks, C. Köberle, C. Haas, and J. A. Hölemann (2013), A combined approach of remote sensing and airborne electromagnetics to determine the volume of polynya sea ice in the Laptev Sea (vol 7, pg 947, 2013), *CRYOSPHERE*, *7*(4), 1107–1108, doi:10.5194/tc-7-1107-2013.

Reimnitz, E., D. Dethleff, and D. Nurnberg (1994), Contrasts IN Arctic shelf sea-ice regimes and some implications - Beaufort Sea versus Laptev Sea, *Marine Geology*, *119*(3-4), 215–225, doi:10.1016/0025-3227(94)90182-1, 4th International Conference on Paleoceanography (ICP IV), KIEL, Germany, Sep. 21-25, 1992.

Romanov, I. (2004), Morphometric Characteristics of Ice and Snow in the Arctic Basin: Aircraft Landing Observations from the Former Soviet Union, 1928-1989, *National Snow and Ice Data Center, Boulder, CO, digital media.[Available online at http://nsidc.org/data/g02140. html.]*.

Rozman, P., J. Hölemann, T. Krumpen, R. Gerdes, C. Köberle, T. Lavergne, S. Adams, and F. Girard-Ardhuin (2011), Validating satellite derived and modelled sea-ice drift in the laptev sea with in situ measurements from the winter of 2007/08, *Polar Research*, *30*(0).

Rudels, B., E. P. Jones, L. G. Anderson, and G. Kattner (1994), *On the Intermediate Depth Waters of the Arctic Ocean*, pp. 33–46, American Geophysical Union, doi:10.1029/GM085p0033.

Rudels, B., L. Anderson, and E. Jones (1996), Formation and evolution of the surface mixed layer and halocline of the Arctic Ocean, *Journal of Geophysical Research*, *101*(C4), 8807–8821.

Rudels, B., E. P. Jones, U. Schauer, and P. Eriksson (2004), Atlantic sources of the arctic ocean surface and halocline waters, *Polar Research*, *23*(2), 181–208, doi:10.1111/j.1751-8369.2004.tb00007.x.

Saha, S., S. Moorthi, H.-L. Pan, X. Wu, J. Wang, S. Nadiga, P. Tripp, R. Kistler, J. Woollen, D. Behringer, H. Liu, D. Stokes, R. Grumbine, G. Gayno, J. Wang, Y.-T. Hou, H.-Y. Chuang, H.-M. H. Juang, J. Sela, M. Iredell, R. Treadon, D. Kleist, P. Van Delst, D. Keyser, J. Derber, M. Ek, J. Meng, H. Wei, R. Yang, S. Lord,

H. Van den Dool, A. Kumar, W. Wang, C. Long, M. Chelliah, Y. Xue, B. Huang, J.-K. Schemm, W. Ebisuzaki, R. Lin, P. Xie, M. Chen, S. Zhou, W. Higgins, C.-Z. Zou, Q. Liu, Y. Chen, Y. Han, L. Cucurull, R. W. Reynolds, G. Rutledge, and M. Goldberg (2010), The ncep climate forecast system reanalysis, *BULLETIN OF THE AMERICAN METEOROLOGICAL SOCIETY*, *91*(8), 1015–1057, doi:10.1175/2010BAMS3001.1.

Smolyanitsky, V., V. Borodachev, A. Mahoney, F. Fetterer, and R. Barry (2007), Sea ice charts of the Russian Arctic in gridded format, 1933-2006, *Colorado USA: National Snow and Ice Data Center*, doi:10.7265/N5D21VHJ.

Steele, M., and T. Boyd (1998), Retreat of the cold halocline layer in the Arctic Ocean, *Journal of Geophysical Research*, *103*(C5), 10,419.

Steele, M., R. Morley, and W. Ermold (2001), Phc: A global ocean hydrography with a high-quality arctic ocean, *Journal of Climate*, *14*, 2079–2087, doi:10.1175/1520-0442(2001)014¡2079:PAGOHW¿2.0.CO;2.

Stevens, D. (1991), The open boundary condition in the United Kingdom fine-resolution Antarctic model, *Journal of Physical Oceanography*, *21*(9), 1494–1499.

Stroeve, J. C., V. Kattsov, A. Barrett, M. Serreze, T. Pavlova, M. Holland, and W. N. Meier (2012), Trends in arctic sea ice extent from cmip5, cmip3 and observations, *Geophysical Research Letters*, *39*(16), doi:10.1029/2012GL052676.

Tremblay, L.-B., and M. Hakakian (2006), Estimating the sea ice compressive strength from satellite-derived sea ice drift and ncep reanalysis data, *Journal of Physical Oceanography*, *36*, 2165–2172, doi:10.1175/JPO2954.1.

Weiss, J. (2013), Sea ice fracturing, in *Drift, Deformation, and Fracture of Sea Ice*, Springer Briefs in Earth Sciences, pp. 53–72, Springer Netherlands, doi:10.1007/978-

94-007-6202-2-4.

Willmes, S., S. Adams, D. Schroeder, and G. Heinemann (2011), Spatio-temporal variability of polynya dynamics and ice production in the Laptev Sea between the winters of 1979/80 and 2007/08, *POLAR RESEARCH*, *30*, doi:10.3402/polar.v30i0.5971.

Winsor, P., and G. Björk (2000), Polynya activity in the Arctic Ocean from 1958 to 1997, *Journal of Geophysical Research-Oceans*, *105*(C4).

Yu, Y., H. Stern, C. Fowler, F. Fetterer, and J. Maslanik (2014), Interannual variability of Arctic landfast ice between 1976 and 2007, *Journal of Climate*, *27*, 227–243, doi:10.1175/JCLI-D-13-00178.1.

Zhang, J., and W. Hibler III (1997), On an efficient numerical method for modeling sea ice dynamics, *Journal of Geophysical Research. C. Oceans*, *102*, 8691–8702.

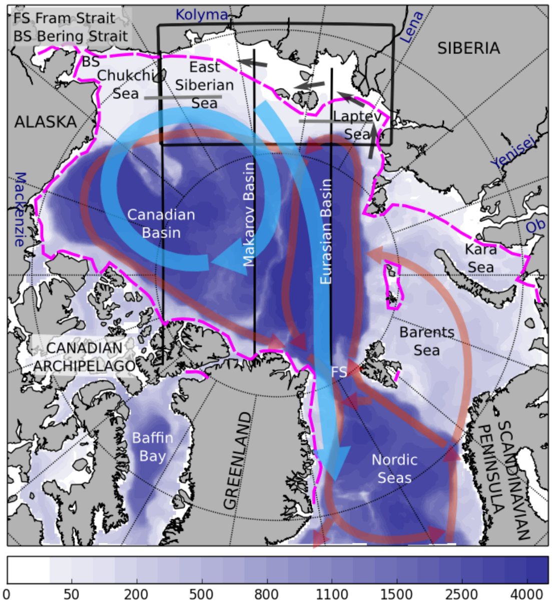

Figure 1. The Arctic Ocean and its marginal seas. The sea ice and surface circulation is schematically represented by light blue and mid-depth circulation by red arrows (simplified from *Rudels et al.* [1994]), respectively. The landfast ice edge is depicted by the magenta dash line. The coastal current in the Laptev and East Siberian Seas is schematically represented by the black arrows. The black lines and box mark the sections and regions used in the model analysis.

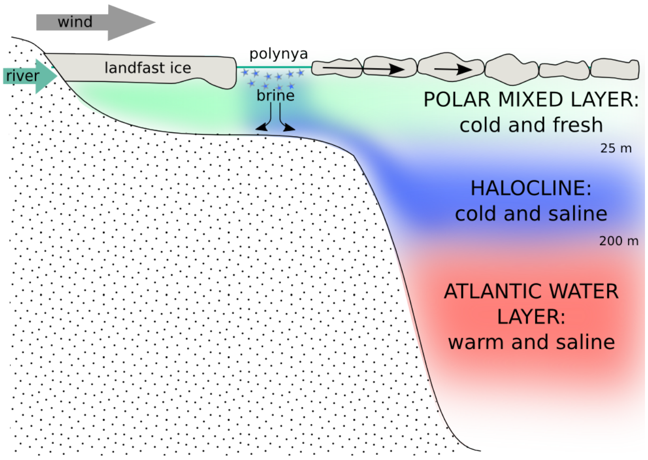

Figure 2. Arctic Ocean vertical stratification and winter processes maintaining the Arctic halocline.

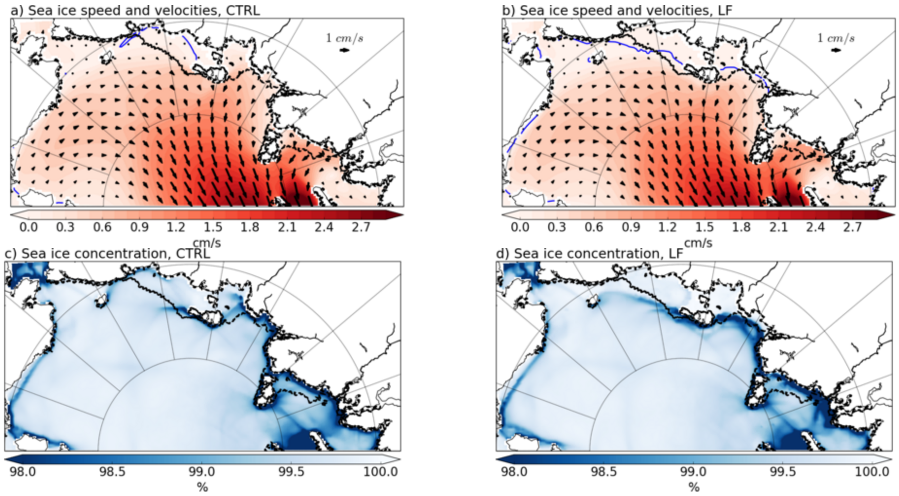

Figure 3. The effect of the landfast ice parametrization on the mean April (2000-2010) sea ice concentration (a,b) and motion (c,d). a,c - CTRL, b,d - LF. Speed 1 mm/s is contoured by blue line. Mean April landfast edge from the AARI dataset (1997-2006) is depicted by gray dash line.

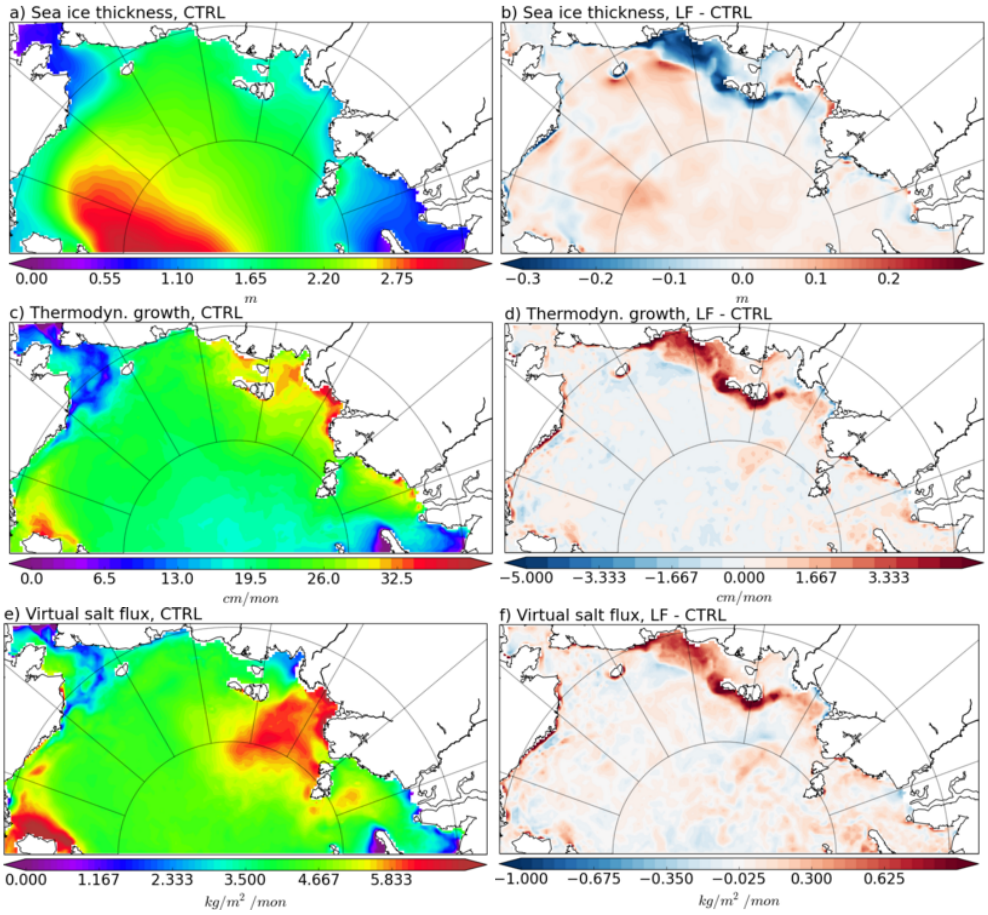

Figure 4. Mean winter (2000-2010) sea ice thickness, thermodynamical growth and salt flux from the sea ice thermodynamical growth: a - CTRL, b - LF minus CTRL.

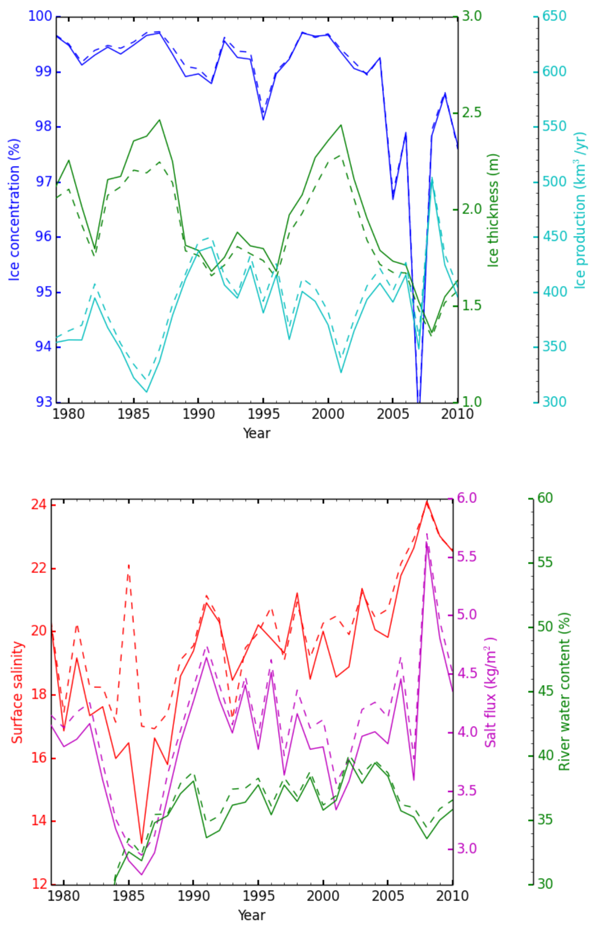

Figure 5. Mean winter (December-April) sea ice time series for the Laptev Sea and East Siberian Sea. CTRL and LF are represented by solid and dash lines, respectively: a - mean sea ice concentration and thickness with total sea ice production; b - sea surface salinity of the areas with the production higher than 30 cm, salt flux resulting from the production and river water content.

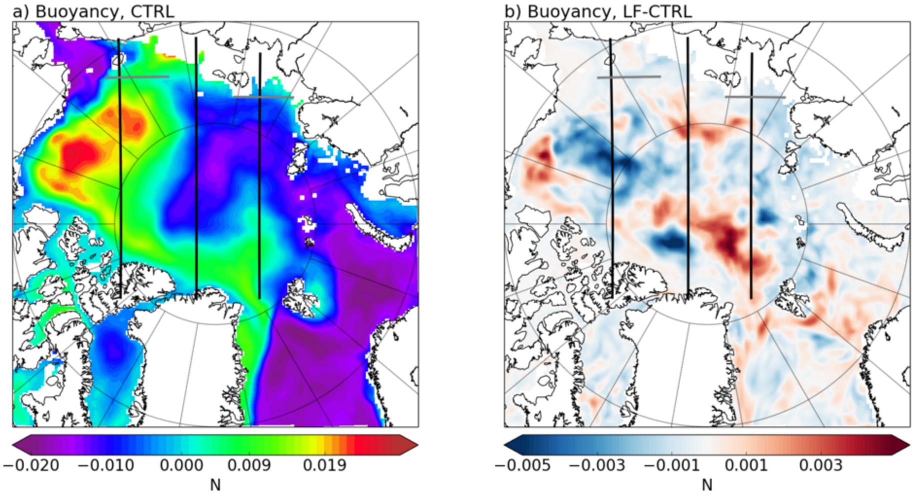

Figure 6. Mean April (2000-2010) buoyancy at the top halocline (25-30 m): a - CTRL, b - LF minus CTRL. Black lines mark the profile sections across Canadian, Makarov and Eurasian Basins (Figs. 7, 9, and 10). Gray line marks a section for the time series at the Eurasian shelf break (Fig. 8).

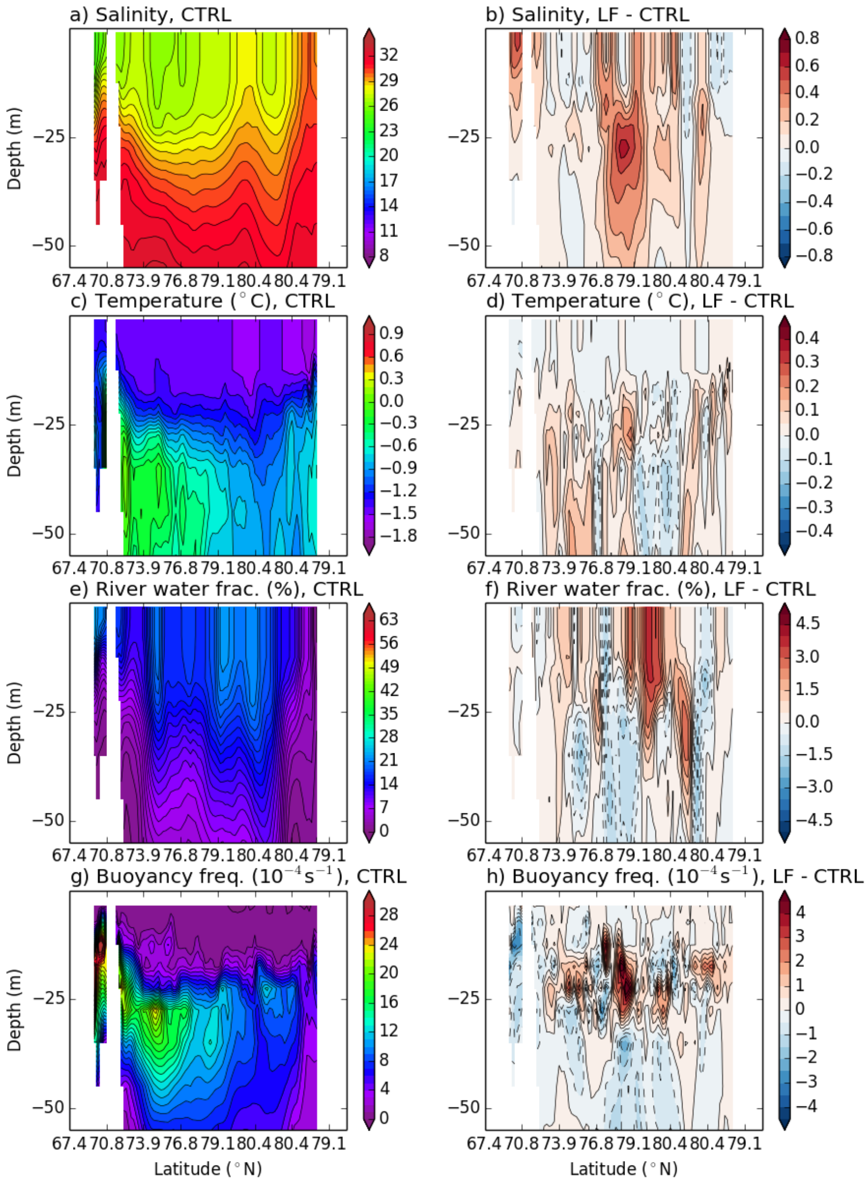

Figure 7. Mean April (2000-2010) salinity, temperature, river water fraction and buoyancy frequency along the section across the Canadian Basin.

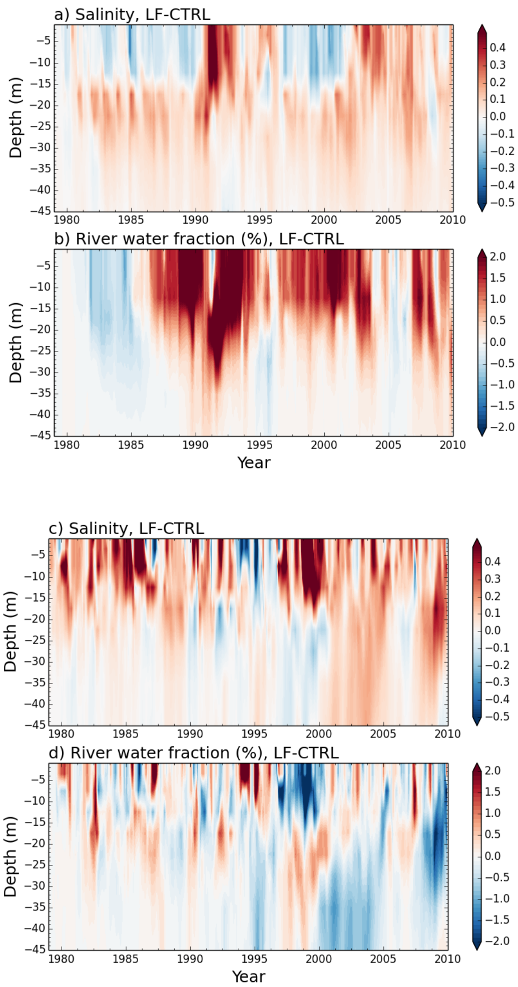

Figure 8. Hovmöller diagrams of monthly mean salinity and river water fraction differences between LF and CTRL: average over an oceanographic section at the Eurasian shelf break north of the East Siberian Sea (a,b) and at the Laptev Sea shelf break (c,d). Sections are marked by gray lines on Fig. 1 and 6.)

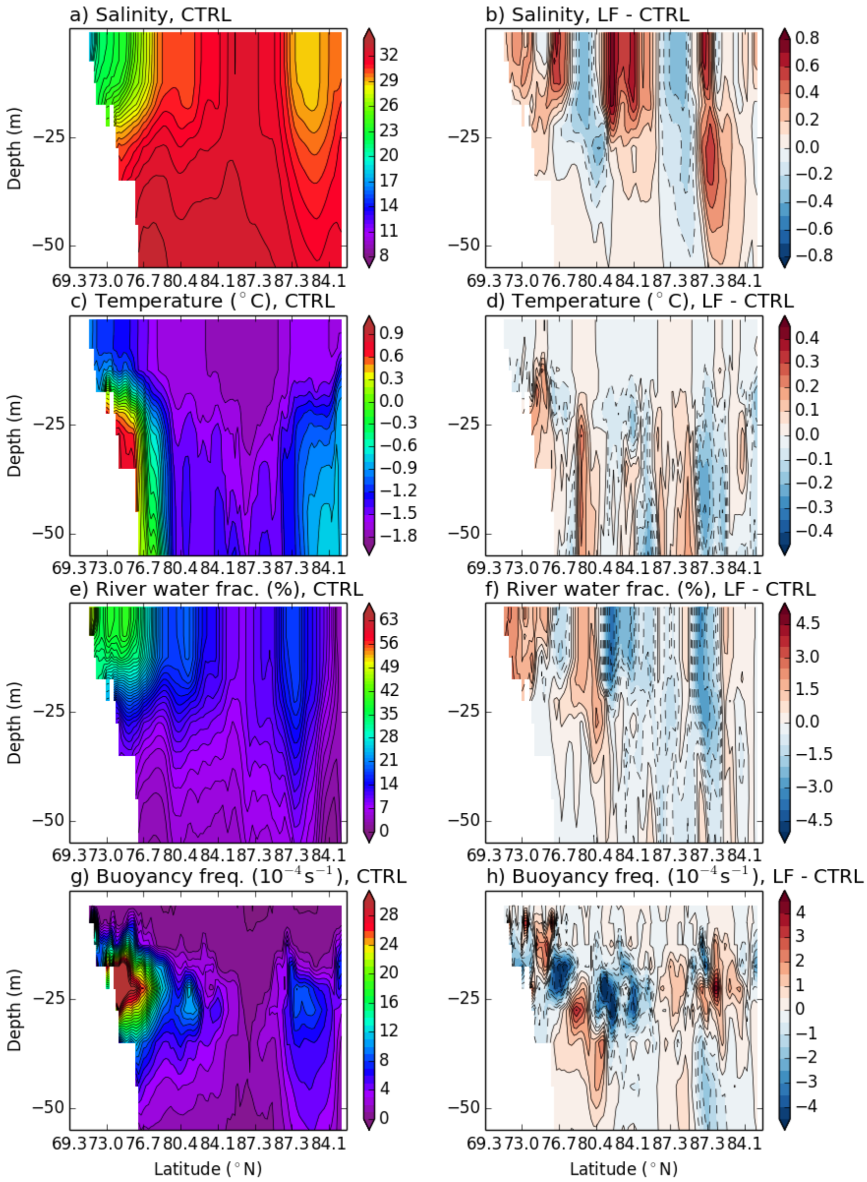

Figure 9. Mean April (2000-2010) salinity, temperature, river water fraction and buoyancy frequency along the section across the Makarov Basin

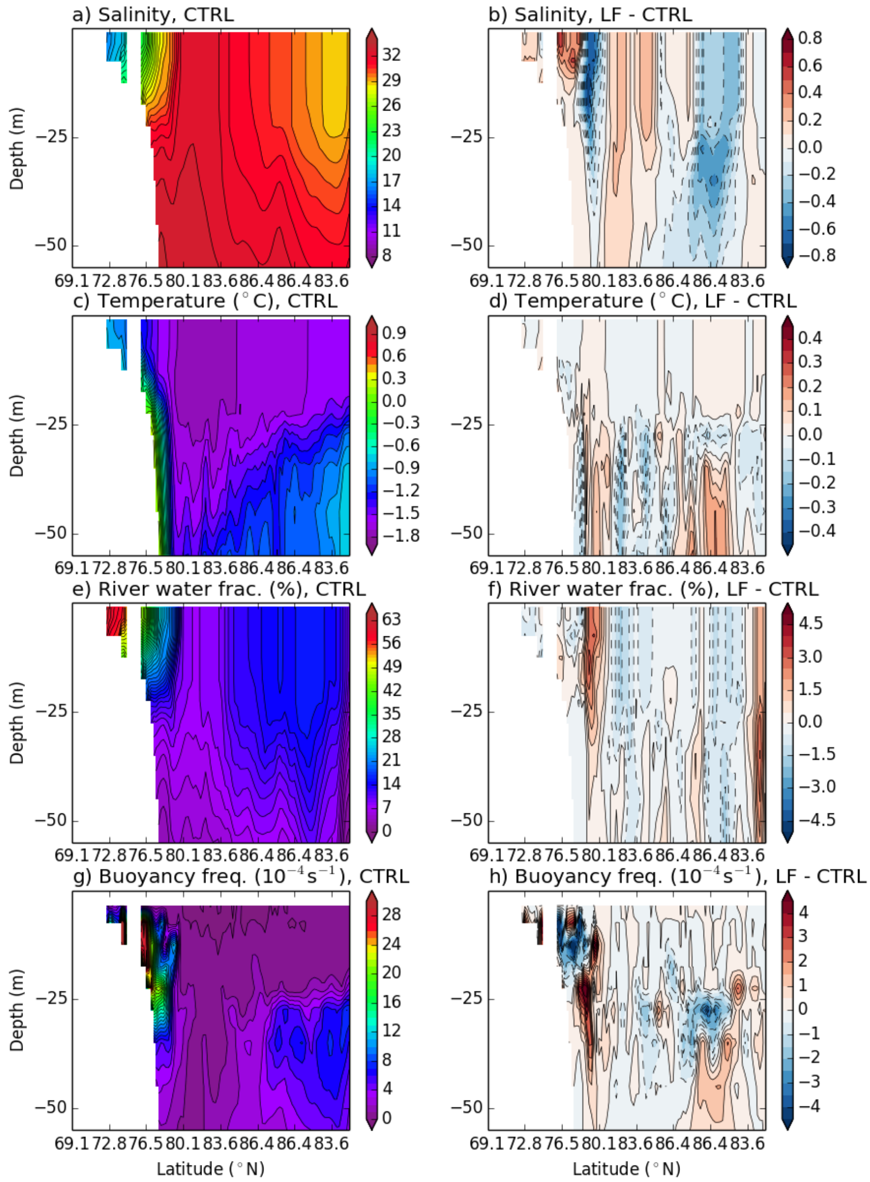

Figure 10. Mean April (2000-2010) salinity, temperature, river water fraction and buoyancy frequency along the section across the Eurasian Basin.